Aerospace Science and Technology 151 (2024) 109341

Contents lists available at ScienceDirect

Aerospace Science and Technology

journal homepage: www.elsevier.com/locate/aescte

Helicopter rotor in a propeller slipstream: Aerodynamic and rotor blade flapping responses

Berend G. van der Wall *

German Aerospace Center (DLR), Institute of Flight Systems, Lilienthalplatz 7, 38110 Braunschweig, Germany

ARTICLE INFO

Keywords:
Helicopter
Aerodynamic interaction
Propeller-rotor interaction
Rotor trim
Rotor blade flapping

ABSTRACT

During helicopter air-to-air refueling the helicopter's rotor can engage the tanker aircraft's wing and flap end tip vortices and the slipstream of its propellers. The tip vortices represent a swirl around an axis that is essentially parallel to the rotor longitudinal axis. The slipstream of the propellers includes a strong air jet downstream that can cover a significant amount of the helicopter's main rotor. This phenomenon was recently treated analytically for a rigid rotor by means of blade-element momentum theory and the rotor control angles required to reject the disturbance were computed. In this article, the rotor blade flapping is introduced as degree of freedom. It is shown that the rotor coning is affected by the slipstream position with respect to the rotor hub. Without retrim, the largest amount of coning and cyclic flapping occurs for slipstream positions on the retreating side of the rotor.

1. Introduction

Helicopter air-to-air refueling (HAAR) was first demonstrated in 1966 with a tanker aircraft driven by propellers and flying at low speed with flaps deployed, while the helicopter was in a high-speed configuration to catch up with the aircraft, Ref. [1]. Today, the situation is unchanged. Helicopter pilots experience high workload i.e. due to multiple sources of air turbulence caused by vortices trailed from the tanker aircraft's wing tips and either ends of the flaps. The helicopter rotor may also encounter the wake of the wing including the shed turbulent boundary layers of upper and lower surfaces. Finally, the propeller's strong air jet and swirl within their slipstream can also engage with the rotor. Investigations so far mainly focused on handling qualities and control laws, Ref. [2], although the various physical sources of these turbulences were known. A literature survey of aircraft air-to-air refueling is given in [3], mentioning HAAR as an essentially military application and potentially of interest for search and rescue missions in civil use cases.

Recently, DLR completed the project F(AI)^{2}R (Future Air-to-Air Refueling) that also included HAAR configurations in trials on DLR's motion-based air vehicle simulator, Ref. [4]. In order to include the aircraft and propeller turbulences at least in a quasi-steady manner, a computational fluid dynamics (CFD) flow field was computed with an aircraft of the size of an Airbus A400M was trimmed to level flight at low speed, with deployed flaps. Its propellers were represented by actuator disks, Ref. [5]. Due to the actuator disk boundary conditions the swirl in the propeller slipstream was also contained. This high-resolution flow field, of which a slice through the inner propeller is shown in Fig. 1, was time-averaged and a raster for real-time simulation was extracted. A grid of 1 m x 0.5 m x 0.5 m (in *x, y* and *z* direction) in space served as air disturbance field for a CH53-size helicopter operating in it.

It can be seen from Fig. 1 (horizontal velocities relative to the speed of flight are shown color-coded) that the propeller slipstream (in yellow) extends downstream up to the tail plane where the helicopter would be located for refueling. Therefore, the helicopter rotor can experience additional peak velocities of up to 34 m/s, at a flight speed of ca. 66 m/s, totaling to 100 m/s over those parts of the rotor disk entrained into the propeller slipstream. Note that the never-exceed flight speed of the CH53 is about 82 m/s. In terms of rotor advance ratio, the flight speed represents a tip speed ratio of ca. $\mu = V_\infty/(\Omega R) \approx 0.31$, while the effective advance ratio within the propeller slipstream could result in a local tip speed ratio of ca. 0.47. Based on the propeller data of Table 1 and rotor data of Table 2 in the Appendix, this disturbance would happen within a strip of a width nearly half of the helicopter rotor radius.

The isolated problem of the aircraft wing tip (or flap tip) vortices immersed in a helicopter's main rotor was solved analytically for the first time in 2017, Ref. [6]. The analytical solution of the propeller slipstream – rotor trim problem was recently solved for a rotor with rigid blades and a slipstream without swirl, Ref. [7]. In this article, the following extensions related to this propeller-rotor interaction

* Corresponding author.
E-mail address: berend.vanderwall@dlr.de.

https://doi.org/10.1016/j.ast.2024.109341
Received 25 April 2024; Received in revised form 17 June 2024; Accepted 18 June 2024
Available online 18 June 2024

Nomenclature

Symbols

a_{ij}	system matrix elements
$\mathbf{A}$, $\mathbf{B}$	system, excitation matrix
b_{ij}	excitation matrix elements
a_∞	speed of sound, m/s
c	rotor blade chord, m
c_μ	advance ratio term, $c_\mu = 2\mu_0 + \Delta\mu$
$C_{l\alpha}$	lift curve slope
C_{Mx}	aerodynamic rolling moment coefficient, $C_{Mx} = M_x / \left(\rho\pi R^2(\Omega R)^2 R\right)$
C_T	rotor thrust coefficient, $C_T = T/\left(\rho\pi R^2(\Omega R)^2\right)$
dC_T	blade element contribution to the thrust coefficient
g	gravitational constant, $g = 9.81$ m/s^2
h	height above sea level, m
m	vehicle mass, kg
M	Mach number, $M = V/a_\infty$
N_b	number of blades
r	non-dimensional radial coordinate, referenced to R
R	rotor or slipstream radius, m
$\vec{u}$	excitation vector
U_T	non-dimensional tangential velocity, referenced to ΩR
U_P	non-dimensional perpendicular velocity, referenced to ΩR
v, V	velocity, m/s
x, y	non-dimensional rotor longitudinal, lateral coordinate
α	angle of attack, deg
β	flapping angle, deg
Δ	perturbation
$\Delta_{\mu\lambda}$	mixed term of advance ratio and inflow perturbations, $\Delta_{\mu\lambda} = \mu_0\Delta\lambda + \lambda\Delta\mu$
ϵ	glide ratio
Θ	blade pitch angle, deg
λ	total inflow ratio, $\lambda = \lambda_i + \mu_z$
λ_C	propeller axial inflow ratio, $\lambda_C = V_\infty/(\Omega R)_p$
λ_i	induced inflow ratio, $\lambda_i = v_i/(\Omega R)$
μ_∞	tip speed ratio, $\mu_\infty = V_\infty/(\Omega R)$
μ	advance ratio, $\mu = \mu_\infty \cos\alpha_S$
μ_z	inflow ratio, $\mu_z = -\mu_\infty \sin\alpha_S$
ρ	air density, kg/m^3
σ	rotor solidity, $\sigma = N_b c/(\pi R)$
ψ	azimuth angle, deg
Ω	rotor rotational speed, rad/s

Subscripts

airc, *hel*, *p*	aircraft, helicopter, propeller
beg, *end*	begin and end of azimuth region
C, *S*	cosine, sine component
h	hover
i	induced
NE	never exceed
p	propeller
S	rotor shaft
tip	blade tip
tw	blade twist
up, *low*	upper and lower radial integration bound
z	*z*-direction
0	undisturbed rotor trim value, mean value
1, 2	left and right end of slipstream
75	at 75 % radius
∞	values of the operational condition

Abbreviations

BEMT	Blade element momentum theory
CFD	Computational fluid dynamics
F(AI)^{2}R	Future Air-to-Air Refueling (DLR project)
HAAR	Helicopter Air-to-Air Refueling

configuration will be addressed that so far have not been published:

- introduction of the flapping degree of freedom,
- trim in undisturbed air with rotor blade flapping included,
- disturbance of the trim condition and the flapping motion by the propeller slipstream,
- the rotor blade pitch control angles required to retrim the rotor and to reject the disturbance impact on harmonic blade flapping.

2. Analysis method

The approach follows the one of Ref. [7], now enhanced by the blade

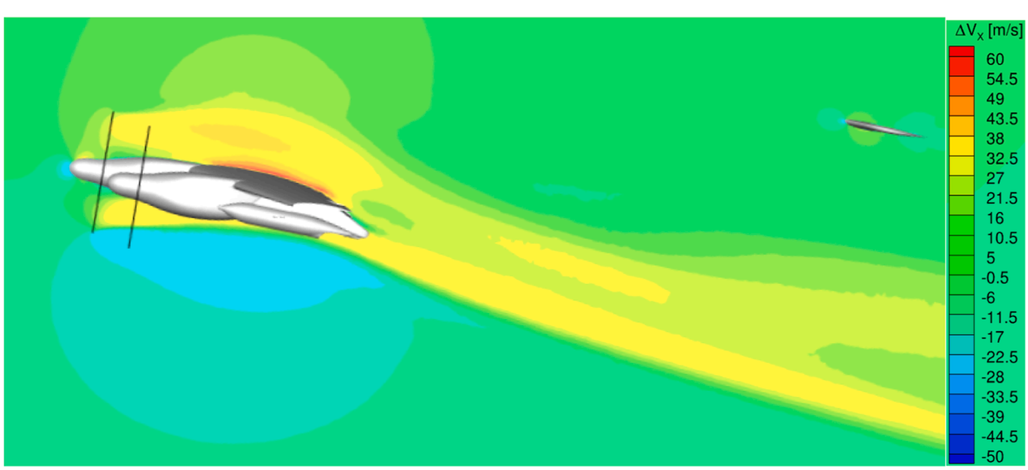

Fig. 1. Horizontal velocities induced by wing and propeller slipstream. Source: P. Löchert.

flapping motion, which for flight mechanical purposes is limited to its mean value (coning) and 1/rev cyclic motion. Higher harmonics do not contribute to the steady rotor thrust and hub moments and are therefore ignored. Simple momentum theory is applied to the propeller in order to compute its induced velocity within the homogenous slipstream (without swirl) and to evaluate the fully developed slipstream contraction radius far behind the propeller as given in Ref. [8].

The helicopter rotor analysis is based on blade element momentum theory (BEMT) as outlined in the classical literature, e.g. Ref. [9], with the usual simplifications such as linear steady incompressible aerodynamics, constant inflow over the disk, and no root or tip losses. The rotor blades are hinged at a small offset from the hub center for simplicity, have a homogenous mass distribution, and only the rigid blade motion in flapping is considered. For evaluation of the mean (coning) and harmonic flapping at the first harmonic (tip path plane longitudinal and lateral tilt) the harmonic balance method is used. Results are computed for the configuration and operational condition mentioned above. Technical data of the tanker aircraft given in Table 1, data of the helicopter in Table 2, and data for a typical HAAR operational condition, based on an aircraft trim with CFD that provided the propeller thrust, in Table 3; all tables are given in the Appendix.

2.1. Propeller slipstream: induced velocity and contraction radius

Applied to the propeller, momentum theory first leads to its induced velocity in the propeller disk at rest v_{hp}, Eq. (1). Next, the introduction of the axial advance ratio $\overline{\lambda_C} = V_\infty/(2v_{hp})$ results in a significant reduction of it to v_{ip}, for details see Ref. [9]. Far from the propeller, in its fully contracted slipstream, twice of this value is the velocity perturbation that will hit the helicopter rotor at a downstream position. For the rotor this represents an additional local tip speed ratio $\Delta\mu_\infty = 2v_{ip}/(\Omega R)$. $\overline{\lambda_C}$ as well defines the contracted radius, which for convenience will be related to the helicopter rotor radius in the form R_∞/R, as derived in Ref. [8]. For this configuration and operational condition, the contracted radius is about 92 % of the propeller radius, therefore the width of the slipstream within the rotor disk amounts to 44.8 % of the helicopter rotor radius, based on the data of Table 1 to Table 3. Also, the advance ratio perturbation (in the plane of the rotor disk) amounts to $\Delta\mu = 0.128$ and the axial inflow ratio perturbation within the slipstream (normal to the rotor disk) becomes $\Delta\mu_z = 0.0266$, due to the nose-down inclination of the rotor shaft, α_S. All the above is summarized in Eq. (1) and data obtained for the operational condition are given in Table 4 in the Appendix.

$$
\begin{gathered}
v_{hp} = \sqrt{\frac{T_p}{2\rho\pi R_p^2}}; \quad \lambda_{hp} = \frac{v_{hp}}{\Omega_p R_p}; \quad \overline{\lambda_C} = \frac{V_\infty}{2v_{hp}}; \quad v_{ip} = v_{hp}\left(\sqrt{\overline{\lambda_C}^2+1} - \overline{\lambda_C}\right) \\
\Delta V_\infty = 2v_{ip}; \quad \Delta\mu_\infty = \frac{\Delta V_\infty}{\Omega R}; \quad \Delta\mu = \Delta\mu_\infty \cos\alpha_S; \quad \Delta\mu_z = -\Delta\mu_\infty \sin\alpha_S \\
\frac{R_\infty}{R_p} = \sqrt{\frac{\overline{\lambda_C} + \sqrt{\overline{\lambda_C}^2+1}}{2\sqrt{\overline{\lambda_C}^2+1}}}; \quad \Delta y = \frac{2R_\infty}{R} = y_2 - y_1
\end{gathered} \tag{1}
$$

In Fig. 2 a sketch is shown with two propeller positions, one on the advancing side and one on the retreating side of the rotor. The slipstream center position y_p and the width $\Delta y = y_2 - y_1$ defined by either end of it. All coordinates x, y are nondimensionalized by the rotor radius R.

2.2. Helicopter rotor: velocities acting on the blades and rotor trim

In this flight condition, shown by Fig. 2, the propeller slipstream leads to increased dynamic pressure on the advancing side of the rotor and to a larger rotor inflow ratio $\Delta\mu_z$. A propeller slipstream acting on the retreating side leads to a significant reduction of dynamic pressure. Also, the reversed flow area is increased as indicated in Fig. 2. The increased inflow ratio therefore leads to significantly larger variations in the blade element angle of attack, compared to the advancing side.

The helicopter rotor is treated by BEMT as outlined in the classical literature, e.g. Ref. [9]. As for the propeller, the rotor's thrust-induced velocity in undisturbed air and its trim to thrust and zero hub moments needs to be evaluated, before the propeller slipstream is included. Note that from Fig. 2, all slipstream perturbations $\Delta\mu$, $\Delta\mu_z$ only act in a strip occupied by the propeller's slipstream, oriented parallel to the rotor's x-axis between y_1 and y_2. Therefore, the velocity components at the blade elements consist of a contribution from flight in undisturbed air present all over the disk (indicated by the subscript 0), plus a perturbation due to the propeller slipstream (indicated by the Delta Δ).

The blade pitch angle consists of a built-in linear twist distribution (with zero twist at 75 % radius), the collective control angle and the longitudinal and lateral cyclic control angles. A trim is done to the steady operational condition as defined in Table 3 initially without flapping motion (with results from Ref. [7]), then with inclusion of flapping. Because the trim is defined for zero 1/rev flapping motion (equivalent to zero hub moments), only blade coning remains.

In the following Eq. (2), the nondimensional velocity components U acting at the blade elements tangential to the rotor plane of rotation (subscript T) and perpendicular to it (subscript P) are given. The blade

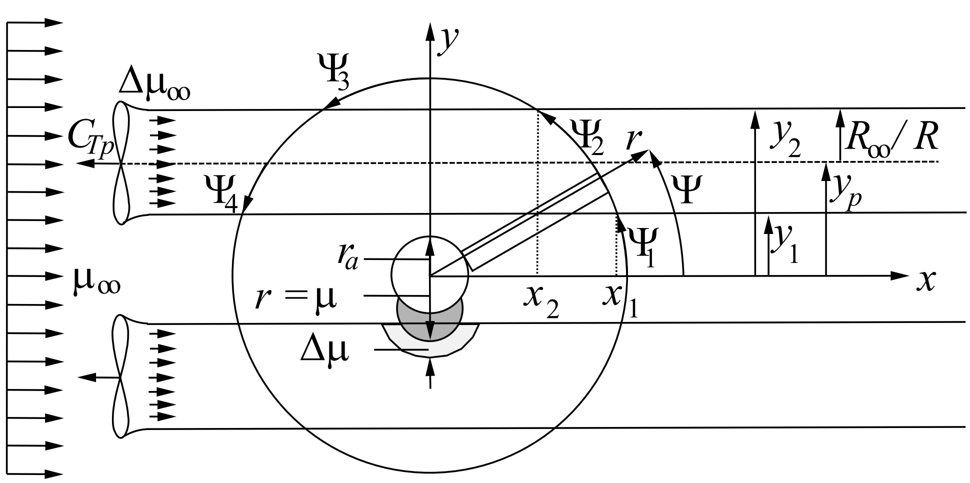

Fig. 2. Sketch of a rotor immersed in the stream tubes of two propellers.

flapping angle β consists of a mean value β_0 (coning angle) and the longitudinal and lateral flapping angles β_c, β_s. Flapping perturbations $\Delta\beta$ and their nondimensional time derivatives are needed. The blade pitch angle Θ_0 for rotor trim in undisturbed air and its perturbations $\Delta\Theta$ needed to retrim the rotor are given. All these contribute to the blade element aerodynamic angle of attack α. Components related to the undisturbed air are acting throughout the entire disk (subscript 0) and the perturbations in the advance ratio and inflow ratios $\Delta\mu, \Delta\mu_z, \Delta\lambda_i$ are acting only in the strip covered by the propeller slipstream. Trim to zero flapping also eliminates all time derivatives of the basic flapping motion in undisturbed air, i.e. $\beta_S = \beta_C = 0$.

$$
\begin{aligned}
U_T &= \underbrace{(r + \mu_0 \sin\psi)}_{U_{T0}} + \underbrace{(\Delta\mu \sin\psi)}_{\Delta U_T} \\
U_P &= \underbrace{\underbrace{(\mu_{z0} + \lambda_{i0})}_{\lambda_0} + \underbrace{\mu_0 \beta_{00} \cos\psi + r\overset{*}{\beta}_{00}}_{U_{P,\beta}}}_{U_{P0}} \\
&+ \underbrace{\underbrace{(\Delta\mu_z + \Delta\lambda_i)}_{\Delta\lambda} + \underbrace{[(\mu_0 + \Delta\mu)\Delta\beta + \Delta\mu\beta_{00}]\cos\psi + r\Delta\overset{*}{\beta}}_{\Delta U_{P,\beta}}}_{\Delta U_P} \\
\beta &= \underbrace{(\beta_0 + \beta_S \sin\psi + \beta_C \cos\psi)}_{\beta_{00} \equiv \beta_0} + \underbrace{(\Delta\beta_0 + \Delta\beta_S \sin\psi + \Delta\beta_C \cos\psi)}_{\Delta\beta} \\
\overset{*}{\beta} &= \underbrace{(\beta_S \cos\psi - \beta_C \sin\psi)}_{\overset{*}{\beta}_{00} = 0} + \underbrace{(\Delta\beta_S \cos\psi - \Delta\beta_C \sin\psi)}_{\Delta\overset{*}{\beta}} \\
\Theta &= \underbrace{(\Theta_{tw} r + \Theta_{root} + \Theta_S \sin\psi + \Theta_C \cos\psi)}_{\Theta_0} + \underbrace{(\Delta\Theta_{75} + \Delta\Theta_S \sin\psi + \Delta\Theta_C \cos\psi)}_{\Delta\Theta} \\
\alpha &= \Theta - \arctan\frac{U_P}{U_T} \approx \Theta_0 + \Delta\Theta - \frac{U_{P0} + \Delta U_P}{U_{T0} + \Delta U_T}
\end{aligned}
\tag{2}
$$

The dynamic pressure in BEMT is based on the tangential velocity U_T only. Then the blade element lift contribution dL and aerodynamic flapping moment dM_β can be computed that are needed for the blade flapping differential equation of motion, Eq. (3). Therein, $\rho, c, R, C_{l\alpha}, \Omega, dr$ are the air density, blade chord length, rotor radius, lift curve slope, and rotor rotational frequency. In the flapping equation of motion, I_β, J_β are the mass moment of inertia and the mass moment associated with centrifugal forces. Superscript dots $\ddot{x}$ indicate a derivative with respect to time, d/dt, an asterisk * with respect to nondimensional time, $d/d\psi$, where ψ is the rotor azimuth angle.

$$
\begin{aligned}
U_T^2 \alpha &\approx \underbrace{U_{T0}^2 \Theta_0 - U_{T0} U_{P0}}_{trim} \\
&\underbrace{+ U_{T0}^2 \Delta\Theta + \left(2U_{T0}\Delta U_T + \Delta U_T^2\right)(\Theta_0 + \Delta\Theta) - U_{T0}\Delta U_P - \Delta U_T (U_{P0} + \Delta U_P)}_{perturbation} \\
dL &= \frac{\rho}{2} c R C_{l\alpha} (\Omega R)^2 U_T^2 \alpha \, dr; \qquad dM_\beta = Rr\, dL; \qquad I_\beta \ddot{\beta} + \Omega^2 J_\beta \beta = M_\beta
\end{aligned}
\tag{3}
$$

A trim to zero 1/rev flapping, i.e. zero hub moments, requires $\beta_C = \beta_S = 0$, therefore $\beta_{00} \equiv \beta_0$ and the time derivative is zero as well. The mean flapping angle β_0 contributes $U_{T0} U_{P,\beta} = (r + \mu_0 \sin\psi)\, \mu_0 \beta_0 \cos\psi$ to the term $U_T^2 \alpha$, i.e. it generates only harmonic lift in 1/rev and 2/rev of dL (but no mean lift at 0/rev), and therefore the blade flapping can be ignored in the trimmed rotor thrust computation. The nondimensional flapping equation of motion can be solved easily for the mean flapping angle, with the Lock number γ and the natural frequency of flapping ν_β, which depends on the hinge offset e_β, Eq. (4):

$$
\begin{aligned}
\overset{**}{\beta} + \nu_\beta^2 \beta = \gamma \overline{M}_\beta \quad &\Rightarrow \quad \beta_0 = \frac{\gamma}{\nu_\beta^2} \overline{M}_{\beta,0}; \quad \gamma = \frac{\rho c R^4 C_{l\alpha}}{I_\beta}; \quad \nu_\beta^2 = \frac{J_\beta}{I_\beta} \\
&= 1 + \frac{3}{2} \frac{e_\beta}{1 - e_\beta}
\end{aligned}
\tag{4}
$$

Therein, the nondimensional aerodynamic flapping moment $\overline{M}_\beta$, without 1/rev flapping, i.e. only with β_0, is

$$
\begin{aligned}
\overline{M}_\beta &= \frac{1}{2} \int_0^1 r\left[U_{T0}^2 \Theta_0 - U_{T0} U_{P0}\right] dr \\
&= \frac{1}{2} \int_0^1 r \begin{bmatrix} \left[r^2 + 2r\mu_0 \sin\psi + \left(\mu_0^2/2\right)(1 - \cos 2\psi)\right] \\ \times (\Theta_{tw} r + \Theta_{root} + \Theta_S \sin\psi + \Theta_C \cos\psi) \\ -(r + \mu_0 \sin\psi)(\lambda_0 + \mu_0 \beta_0 \cos\psi) \end{bmatrix} dr
\end{aligned}
\tag{5}
$$

After conversion of multiplication of trigonometric functions into sums of harmonics, all remaining harmonics can be removed due to zero moment trim of the undisturbed rotor (or, mathematically, computation of $\overline{M}_{\beta,0} = 1/(2\pi) \int_0^{2\pi} \overline{M}_\beta d\psi$). The mean, Sine and Cosine moments result in

$$
\begin{aligned}
\overline{M}_{\beta,0} &= \frac{1}{2} \int_0^1 r\left[\left(r^2 + \frac{\mu_0^2}{2}\right)(\Theta_{tw} r + \Theta_{root}) + r\mu_0 \Theta_S - r\lambda_0\right] dr \\
&= \left(\frac{1}{10} + \frac{\mu_0^2}{12}\right)\Theta_{tw} + \frac{1 + \mu_0^2}{8}\Theta_{root} + \frac{\mu_0}{6}\Theta_S - \frac{1}{6}\lambda_0 \quad \Rightarrow \quad \beta_0 = \frac{\gamma}{\nu_\beta^2}\overline{M}_{\beta,0} \\
\overline{M}_{\beta,S} &= \frac{\mu_0}{4}\Theta_{tw} + \frac{\mu_0}{3}\Theta_{root} + \frac{2 + 3\mu_0^2}{16}\Theta_S - \frac{\mu_0}{4}\lambda_0 \\
\overline{M}_{\beta,C} &= \frac{2 + \mu_0^2}{16}\Theta_C - \frac{\mu_0}{6}\beta_0 \quad \Rightarrow \quad \Theta_C = \frac{4\mu_0}{6 + 3\mu_0^2}\beta_0
\end{aligned}
\tag{6}
$$

At the forward blade position the advance ratio generates an upwash at the rotor blade due to the mean flapping angle β_0 (relative to no coning) and hence lift. In its downstream position the coning generates a downwash with associated loss of lift. This results in a Cosine moment at the hub and it requires some Θ_C for compensation of it. A rigid blade with $\beta_0 = 0$ does not generate this upwash/downwash combination and therefore $\Theta_C = 0$. The remaining moment due to the disturbance is periodic at a number of harmonics, but only the constant, 1/rev Sine and Cosine components are of interest for the perturbations of the mean and 1/rev motion of the rotor blade. Expanding the differential equation of motion leads to

$$
\begin{aligned}
\overset{**}{\beta} + \nu_\beta^2 \beta &= -\Delta\beta_S \sin\psi - \Delta\beta_C \cos\psi + \nu_\beta^2(\Delta\beta_0 + \Delta\beta_S \sin\psi + \Delta\beta_C \cos\psi) \\
&= \nu_\beta^2 \Delta\beta_0 + \left(\nu_\beta^2 - 1\right)\Delta\beta_S \sin\psi + \left(\nu_\beta^2 - 1\right)\Delta\beta_C \cos\psi \\
&= \gamma\Delta\overline{M}_{\beta 0} + \gamma\Delta\overline{M}_{\beta S}\sin\psi + \gamma\Delta\overline{M}_{\beta C}\cos\psi \\
\Delta\overline{M}_\beta &= \frac{1}{2}\int_0^1 r\left[U_{T0}^2 \Delta\Theta + \left(2U_{T0}\Delta U_T + \Delta U_T^2\right)(\Theta_0 + \Delta\Theta) - U_{T0}\Delta U_P\right. \\
&\left. - \Delta U_T (U_{P0} + \Delta U_P)\right] dr \\
&= \Delta\overline{M}_{\beta 0} + \Delta\overline{M}_{\beta S}\sin\psi + \Delta\overline{M}_{\beta C}\cos\psi + \Delta\overline{M}_{\beta 2S}\sin 2\psi + \Delta\overline{M}_{\beta 2C}\cos 2\psi + \ldots
\end{aligned}
\tag{7}
$$

For the case of the rotor not being retrimmed to thrust and zero flapping in 1/rev, i.e. $\Delta\Theta = 0$, the resulting development of flapping $\Delta\beta$ is based on the perturbation moments in 0 and 1/rev. The basic equation for the aerodynamic flapping moment without the components of the undisturbed trim $r\left(U_{T0}^2\Theta_0 - U_{T0}U_{P0}\right)$ is

$$\Delta\overline{M}_\beta = \frac{1}{2}\int_0^1 r\left[\left(2U_{T0}\Delta U_T + \Delta U_T^2\right)\Theta_0 - U_{T0}\Delta U_P - \Delta U_T(U_{P0}+\Delta U_P)\right] dr \tag{8}$$

Inserting terms from Eq. (2) leads to

$$\Delta\overline{M}_\beta = \frac{1}{2}\int_0^1 r\begin{bmatrix}\Delta\mu(2r\sin\psi+\mu_0-\mu_0\cos2\psi)(\Theta_{tw}r+\Theta_{root}+\Theta_S\sin\psi+\Theta_C\cos\psi)\\ +(\Delta\mu^2/2)(1-\cos2\psi)(\Theta_{tw}r+\Theta_{root}+\Theta_S\sin\psi+\Theta_C\cos\psi)\\ -(r+\mu_0\sin\psi)(\Delta\mu_z+\Delta\lambda_i+\Delta\mu\beta_0\cos\psi)\\ -(r+\mu_0\sin\psi)(\mu_0+\Delta\mu)(\Delta\beta_0+\Delta\beta_S\sin\psi+\Delta\beta_C\cos\psi)\cos\psi\\ -(r+\mu_0\sin\psi)r(\Delta\beta_S\cos\psi-\Delta\beta_C\sin\psi)\\ -(\Delta\mu\sin\psi)(\mu_{z0}+\lambda_{i0}+\mu_0\beta_0\cos\psi)\\ -(\Delta\mu\sin\psi)(\Delta\mu_z+\Delta\lambda_i+\Delta\mu\beta_0\cos\psi)\\ -(\Delta\mu\sin\psi)(\mu_0+\Delta\mu)(\Delta\beta_0+\Delta\beta_S\sin\psi+\Delta\beta_C\cos\psi)\cos\psi\\ -(\Delta\mu\sin\psi)r(\Delta\beta_S\cos\psi-\Delta\beta_C\sin\psi)\end{bmatrix} dr \tag{9}$$

Note that due to the perturbation without retrim the thrust coefficient C_T will change and with it the induced inflow λ_{i0} on the entire disk and the mean flapping angle β_0 following Eq. (6) must be newly computed. A further change of the inflow ratio $\Delta\lambda_i$ is present only within the perturbation zone due to the increased advance ratio therein. When retrimming the rotor, C_T and with it λ_{i0} and β_0 remain unchanged.

$$\lambda_{i0} = \frac{C_T^{(new)}}{2\mu_0};\qquad \Delta\lambda_i = -\frac{C_T^{(new)}}{2\mu_0}\frac{\Delta\mu}{\mu_0+\Delta\mu};\qquad \beta_0 = \frac{\gamma}{\nu_\beta^2}\overline{M}_{\beta,0}^{(new)} \tag{10}$$

As long as the disturbance covers the entire rotor disk the computation of the constant, Sine and Cosine contribution can easily be performed by dual integration over r and ψ in Eq. (7). This is equivalent to a higher advance ratio $\mu = \mu_0 + \Delta\mu$. The equation of motion leads to a system of linearly coupled algebraic equations for $\Delta\beta_0, \Delta\beta_S, \Delta\beta_C$. Even in the case of a retrim to $C_T = const.$ and zero 1/rev flapping, the mean flapping will change by a small amount of $\Delta\beta_0$ due to a change in the center of lift along the blade span.

For a rotor first trimmed in undisturbed flow, then partly immersed into a propeller slipstream, the perturbations of ΔU_T, ΔU_P, $\Delta\lambda_i$ solely occur within a strip of constant width, parallel to the x-axis inside the rotor disk. This complicates the analysis, because the lower and upper radial integration bounds lead to terms with $\sin^{-n}\psi,\ n = 1,2,3,4$ (see Ref. [7]) over a limited range of azimuth. The resulting flapping motion $\Delta\beta$ acts over the entire disk, as do the control angles $\Delta\Theta$ in case of retrimming. The flapping motion $\Delta\beta$ acts on the entire disk and contributes to the overall thrust of the otherwise undisturbed rotor.

$$\begin{aligned}\Delta dC_T(\Delta\beta) &= -\frac{\sigma C_{l\alpha}}{2}U_{T0}\Delta U_{P,\beta}\,dr = -\frac{\sigma C_{l\alpha}}{2}(r+\mu_0\sin\psi)\left(\mu_0\Delta\beta\cos\psi + r\Delta\overset{*}{\beta}\right)dr\\ &= -\frac{\sigma C_{l\alpha}}{2}(r+\mu_0\sin\psi)\begin{bmatrix}\mu_0(\Delta\beta_0+\Delta\beta_S\sin\psi+\Delta\beta_C\cos\psi)\cos\psi\\ +r(\Delta\beta_S\cos\psi-\Delta\beta_C\sin\psi)\end{bmatrix}dr\\ &= -\frac{\sigma C_{l\alpha}}{2}\begin{bmatrix}r^2(\Delta\beta_S\cos\psi-\Delta\beta_C\sin\psi)\\ +r\mu_0(\Delta\beta_0\cos\psi+\Delta\beta_S\sin2\psi+\Delta\beta_C\cos2\psi)\\ +\mu_0^2(\Delta\beta_0\sin2\psi)/2\\ +\mu_0^2[\Delta\beta_S(\cos\psi-\cos3\psi)+\Delta\beta_C(-\sin\psi+\sin3\psi)]/4\end{bmatrix}dr\\ \Delta dC_{Mx}(\Delta\beta) &= r\sin\psi\,\Delta dC_T(\Delta\beta);\qquad \Delta dC_{My}(\Delta\beta) = -r\cos\psi\,\Delta dC_T(\Delta\beta)\end{aligned} \tag{11}$$

As it can be seen, only harmonic components remain in the thrust coefficient and the mean value is zero: $\Delta C_T(\Delta\beta) = 0$. Hence, the thrust is not changed by any kind of flapping developing due to the disturbance, but only by the disturbance itself. The aerodynamic rolling moment will be proportional to $(2+\mu_0^2)\Delta\beta_C/16$ and the pitching moment to $\mu_0\Delta\beta_0/6 + (2+\mu_0^2)\Delta\beta_S/16$.

It remains to compute the flapping motion due to both, (a) the disturbance as excitation and (b) the aerodynamics acting on the blade in the rest of the rotor disk. This is done by evaluating the Fourier coefficients of the aerodynamic flapping moment. Formally, the result can be written as

$$\begin{Bmatrix}\Delta\overline{M}_{\beta0}\\ \Delta\overline{M}_{\beta S}\\ \Delta\overline{M}_{\beta C}\end{Bmatrix} = \begin{bmatrix}a_{11} & a_{12} & a_{13}\\ a_{21} & a_{22} & a_{23}\\ a_{31} & a_{32} & a_{33}\end{bmatrix}\begin{Bmatrix}\Delta\beta_0\\ \Delta\beta_S\\ \Delta\beta_C\end{Bmatrix} + \begin{Bmatrix}c_1\\ c_2\\ c_3\end{Bmatrix} \tag{12}$$

The coefficients c_i are functions of the blade twist, the trim condition (advance ratio, shaft tilt angle, trim control angles) and the perturbations (advance ratio, thrust, inflow ratio). The equation of motion, Eq. (7), then leads to the computation of the blade flapping perturbations.

$$\begin{bmatrix}\nu_\beta^2-\gamma a_{11} & -\gamma a_{12} & -\gamma a_{13}\\ -\gamma a_{21} & \nu_\beta^2-1-\gamma a_{22} & -\gamma a_{23}\\ -\gamma a_{31} & -\gamma a_{32} & \nu_\beta^2-1-\gamma a_{33}\end{bmatrix}\begin{Bmatrix}\Delta\beta_0\\ \Delta\beta_S\\ \Delta\beta_C\end{Bmatrix} = \gamma\begin{Bmatrix}c_1\\ c_2\\ c_3\end{Bmatrix} \tag{13}$$

The aerodynamic flapping moment in Eq. (9) can be split into three contributions:

(a) the part of the trim controls with the new thrust, inflow ratio and mean flapping angle;
(b) the part with flapping perturbation acting over the entire disk in undisturbed flow;
(c) the part acting only in the region of the slipstream with the velocity perturbations.

Due to the change of thrust the mean inflow λ_{i0} and its variation within the region occupied by the slipstream $\Delta\lambda_i$ must be recalculated, following Eq. (10). For (a), with $\Delta\mu = \Delta\mu_z = \Delta\lambda_i = \Delta\beta = 0$ in the rotor disk, the flapping moment due to modified thrust, mean inflow and mean flapping angle becomes

$$\begin{aligned}\Delta\overline{M}_\beta^{(a)} &= \frac{1}{2}\int_0^1 rU_{T0}(U_{T0}\Theta_0 - U_{P0})\,dr\\ &= \frac{1}{2}\int_0^1 r\begin{bmatrix}\left(\mu_0^2/2+r^2+2r\mu_0\sin\psi-\mu_0^2/2\cos2\psi\right)\\ \times(\Theta_{tw}r+\Theta_{root}+\Theta_S\sin\psi+\Theta_C\cos\psi)\\ -(r+\mu_0\sin\psi)\left(\lambda_0^{(new)}+\mu_0\beta_0^{(new)}\cos\psi\right)\end{bmatrix}dr\end{aligned} \tag{14}$$

Expanding the products of trigonometric functions to the individual harmonics results in

$$\Delta\overline{M}_\beta^{(a)} = \frac{1}{2}\int_0^1 r\begin{bmatrix}\left(\mu_0^2/2+r^2\right)(\Theta_{tw}r+\Theta_{root})+r\mu_0\Theta_S-r\lambda_0^{(new)}\\ +\left[2r\mu_0(\Theta_{tw}r+\Theta_{root})+\left(3\mu_0^2/4+r^2\right)\Theta_S-\mu_0\lambda_0^{(new)}\right]\sin\psi\\ +\left[\left(\mu_0^2/4+r^2\right)\Theta_C-r\mu_0\beta_0^{(new)}\right]\cos\psi\\ +\left(r\mu_0\Theta_C-\mu_0^2/2\beta_0^{(new)}\right)\sin2\psi\\ -\left[\mu_0^2/2(\Theta_{tw}r+\Theta_{root})+r\mu_0\Theta_S\right]\cos2\psi\\ -\mu_0^2/4\Theta_S\sin3\psi-\mu_0^2/4\Theta_C\cos3\psi\end{bmatrix}dr \tag{15}$$

After radial integration, the mean and first harmonics of the Fourier series can directly be extracted. Higher harmonics are not required for the rotor trim.

$$\begin{Bmatrix}\Delta\overline{M}_{\beta0}^{(a)}\\ \Delta\overline{M}_{\beta S}^{(a)}\\ \Delta\overline{M}_{\beta C}^{(a)}\end{Bmatrix} = \begin{Bmatrix}\dfrac{6+5\mu_0^2}{60}\Theta_{tw}+\dfrac{1+\mu_0^2}{8}\Theta_{root}+\dfrac{\mu_0}{6}\Theta_S-\dfrac{1}{6}\lambda_0^{(new)}\\ \dfrac{\mu_0}{4}\Theta_{tw}+\dfrac{\mu_0}{3}\Theta_{root}+\dfrac{2+3\mu_0^2}{16}\Theta_S-\dfrac{\mu_0}{4}\lambda_0^{(new)}\\ \dfrac{2+\mu_0^2}{16}\Theta_C-\dfrac{\mu_0}{6}\beta_0^{(new)}\end{Bmatrix} \tag{16}$$

For (b), with $\Delta\mu = \Delta\mu_z = \Delta\lambda_i = 0$ in the rotor disk, the flapping moment due to flapping motion perturbation $\Delta\beta$ becomes

$$\Delta\overline{M}_\beta^{(b)} = -\frac{1}{2}\int_0^1 rU_{T0}\Delta U_{P,\beta}\,dr$$

$$= -\frac{1}{2}\int_0^1 r(r+\mu_0\sin\psi)\begin{bmatrix}\frac{\mu_0}{2}\Delta\beta_C - r\Delta\beta_C\sin\psi + (\mu_0\Delta\beta_0 + r\Delta\beta_S)\cos\psi \\ +\frac{\mu_0}{2}(\Delta\beta_S\sin2\psi + \Delta\beta_C\cos2\psi)\end{bmatrix}dr \tag{17}$$

Expanding the products of trigonometric functions to the individual harmonics results in

$$\Delta\overline{M}_\beta^{(b)} = -\frac{1}{2}\int_0^1\begin{bmatrix}\left(r\frac{\mu_0^2}{4}-r^3\right)\Delta\beta_C\sin\psi + \left[r^2\mu_0\Delta\beta_0 + \left(r\frac{\mu_0^2}{4}+r^3\right)\Delta\beta_S\right]\cos\psi \\ +\left(r\frac{\mu_0^2}{2}\Delta\beta_0 + r^2\mu_0\Delta\beta_S\right)\sin2\psi + r^2\mu_0\Delta\beta_C\cos2\psi \\ +r\frac{\mu_0^2}{4}(\Delta\beta_C\sin3\psi - \Delta\beta_S\cos3\psi)\end{bmatrix}dr \tag{18}$$

After radial integration, the mean and first harmonics of the Fourier series can directly be extracted. Higher harmonics are not required for the rotor trim.

$$\begin{Bmatrix}\Delta\overline{M}_{\beta0}^{(b)} \\ \Delta\overline{M}_{\beta S}^{(b)} \\ \Delta\overline{M}_{\beta C}^{(b)}\end{Bmatrix} = \begin{Bmatrix}0 \\ \frac{2-\mu_0^2}{16}\Delta\beta_C \\ -\frac{\mu_0}{6}\Delta\beta_0 - \frac{2+\mu_0^2}{16}\Delta\beta_S\end{Bmatrix} = \begin{bmatrix}0 & 0 & 0 \\ 0 & 0 & \frac{2-\mu_0^2}{16} \\ -\frac{\mu_0}{6} & -\frac{2+\mu_0^2}{16} & 0\end{bmatrix}\begin{Bmatrix}\Delta\beta_0 \\ \Delta\beta_S \\ \Delta\beta_C\end{Bmatrix} \tag{19}$$

For (c), within the region occupied by the propeller slipstream, the integrals are limited in the range of radial extension and azimuth, see Table 6, Table 7 and Fig. 6 in the Appendix. The integrations can be done analytically, but the computation requires numerical evaluation at the respective upper and lower limits, see Ref. [7]. Within this region the aerodynamic moment, without the contribution of (b), i.e. Eq. (9), Eq. (18), is

$$\Delta\overline{M}_\beta^{(c)} = \frac{1}{2}\int_{r_{low}}^{r_{up}} r\begin{bmatrix}2\left(r\Delta\mu\sin\psi + \frac{\mu_0}{2}\Delta\mu(1-\cos2\psi)\right) \\ \times[\Theta_{tw}(r-0.75)+\Theta_{75}+\Theta_S\sin\psi+\Theta_C\cos\psi] \\ +\frac{\Delta\mu^2}{2}(1-\cos2\psi)[\Theta_{tw}(r-0.75)+\Theta_{75}+\Theta_S\sin\psi+\Theta_C\cos\psi] \\ -(r+\mu_0\sin\psi)\left(\Delta\mu_z+\Delta\lambda_i+\Delta\mu\beta_0^{(new)}\cos\psi\right) \\ -(r+\mu_0\sin\psi)\Delta\mu(\Delta\beta_0+\Delta\beta_S\sin\psi+\Delta\beta_C\cos\psi)\cos\psi \\ -(\Delta\mu\sin\psi)\left(\Delta\mu_z+\Delta\lambda_i+\Delta\mu\beta_0^{(new)}\cos\psi\right) \\ -(\Delta\mu\sin\psi)(\mu_0+\Delta\mu)(\Delta\beta_0+\Delta\beta_S\sin\psi+\Delta\beta_C\cos\psi)\cos\psi \\ -(\Delta\mu\sin\psi)r(\Delta\beta_S\cos\psi-\Delta\beta_C\sin\psi)\end{bmatrix}dr \tag{20}$$

This includes terms independent of the flapping motion, i.e. parts that remain on the right side of Eq. (7) or Eq. (13) and those that include the flapping perturbations and contribute to the coefficients a_{ij} on the left side of Eq. (13). First, the contribution independent of $\Delta\beta$, with $c_\mu = 2\mu_0 + \Delta\mu$ and $\Theta_{root} = \Theta_{75} - 0.75\Theta_{tw}$:

$$\Delta\overline{M}_\beta^{(c1)} = \frac{\Delta\mu}{2}\int_{r_{low}}^{r_{up}}\begin{bmatrix}\frac{c_\mu}{2}\Theta_{root}r + \left(\Theta_S + \frac{c_\mu}{2}\Theta_{tw} - \frac{\Delta\lambda}{\Delta\mu}\right)r^2 \\ +\left[\left(\frac{3}{4}c_\mu\Theta_S - \mu\frac{\Delta\lambda}{\Delta\mu}\right)r + 2\Theta_{root}r^2 + 2\Theta_{tw}r^3\right]\sin\psi \\ +\left(\frac{c_\mu}{4}\Theta_C r - \beta_0^{(new)}r^2\right)\cos\psi + \left(\Theta_C r^2 - \frac{\mu_0}{2}\beta_0^{(new)}r\right)\sin2\psi \\ -\left[\frac{c_\mu}{2}\Theta_{root}r + \left(\Theta_S + \frac{c_\mu}{2}\Theta_{tw}\right)r^2\right]\cos2\psi \\ -\frac{c_\mu}{4}\Theta_S r\sin3\psi - \frac{c_\mu}{4}\Theta_C r\cos3\psi\end{bmatrix}dr \tag{21}$$

Second, the contribution with the perturbation flapping motion $\Delta\beta$:

$$\Delta\overline{M}_\beta^{(c2)} = -\frac{\Delta\mu}{2}\int_{r_{low}}^{r_{up}}\begin{bmatrix}\left(r^2\cos\psi + r\frac{c_\mu}{2}\sin2\psi\right)\Delta\beta_0 \\ +\left(r^2\sin2\psi + r\frac{c_\mu}{4}(\cos\psi - \cos3\psi)\right)\Delta\beta_S \\ +\left(r^2\cos2\psi + r\frac{c_\mu}{4}(\sin\psi + \sin3\psi)\right)\Delta\beta_C\end{bmatrix}dr \tag{22}$$

As before, the mean value, Sine and Cosine parts must be evaluated for the both contributions (c1) and (c2). In contrast to an integration over the entire revolution, the azimuthal and radial integrations are limited to the region affected by the slipstream, that are given in the Appendix. For the mean part:

$$\Delta\overline{M}_{\beta0}^{(c1)} = \frac{1}{2\pi}\sum_{i_{reg}=1}^{N_{reg}}\int_{\psi_{beg}(i_{reg})}^{\psi_{end}(i_{reg})}\frac{\Delta\mu}{2}\left[\begin{matrix}\frac{c_\mu}{4}\Theta_{root}r^2 + \frac{1}{3}\left(\Theta_S + \frac{c_\mu}{2}\Theta_{tw} - \frac{\Delta\lambda}{\Delta\mu}\right)r^3 \\ +\left[\left(\frac{3}{8}c_\mu\Theta_S - \frac{\mu}{2}\frac{\Delta\lambda}{\Delta\mu}\right)r^2 + \frac{2}{3}\Theta_{root}r^3 + \frac{1}{2}\Theta_{tw}r^4\right]\sin\psi \\ +\left(\frac{c_\mu}{8}\Theta_C r^2 - \frac{1}{3}\beta_0 r^3\right)\cos\psi + \left(\frac{1}{3}\Theta_C r^3 - \frac{\mu_0}{4}\beta_0 r^2\right)\sin2\psi \\ -\left[\frac{c_\mu}{4}\Theta_{root}r^2 + \frac{1}{3}\left(\Theta_S + \frac{c_\mu}{2}\Theta_{tw}\right)r^3\right]\cos2\psi \\ -\frac{c_\mu}{8}\Theta_S r^2\sin3\psi - \frac{c_\mu}{8}\Theta_C r^2\cos3\psi\end{matrix}\right]_{r_{low}(i_{reg})}^{r_{up}(i_{reg})}d\psi \tag{23}$$

As in Ref. [7], the various cases and the different regions within each case have different radial boundaries. This encompasses values of 0, $y_1/\sin\psi$, $y_2/\sin\psi$ and 1 to the powers from 2 to 4. Only contributions symmetric to the y-axis contribute to the mean value; all others cancel each other. Terms containing $\cos\psi, \sin2\psi, \cos3\psi, \sin4\psi$ can be removed. The same is true for the Sine component (respectively, the lateral flapping moment).

$$\Delta\overline{M}_{\beta 0}^{(c1)} = \frac{1}{2\pi}\sum_{i_{reg}=1}^{N_{reg}} \int_{\psi_{beg}(i_{reg})}^{\psi_{end}(i_{reg})} \frac{\Delta\mu}{2} \left[\begin{array}{l} \frac{c_\mu}{4}\Theta_{root}r^2 + \frac{1}{3}\left(\Theta_S+\frac{c_\mu}{2}\Theta_{tw}-\frac{\Delta\lambda}{\Delta\mu}\right)r^3 \\ +\left[\left(\frac{3}{8} c_\mu\Theta_S - \frac{\mu}{2}\frac{\Delta\lambda}{\Delta\mu}\right)r^2+\frac{2}{3}\Theta_{root}r^3+\frac{1}{2}\Theta_{tw}r^4\right]\sin\psi \\ -\left[\frac{c_\mu}{4}\Theta_{root}r^2+\frac{1}{3}\left(\Theta_S+\frac{c_\mu}{2}\Theta_{tw}\right)r^3\right]\cos2\psi \\ -\frac{c_\mu}{8}\Theta_S r^2\sin3\psi \end{array}\right]_{r_{low}(i_{reg})}^{r_{up}(i_{reg})} d\psi \qquad (24)$$

The lateral flapping moment contribution therefore becomes

$$\Delta\overline{M}_{\beta S}^{(c1)} = \frac{1}{\pi}\sum_{i_{reg}=1}^{N_{reg}} \int_{\psi_{beg}(i_{reg})}^{\psi_{end}(i_{reg})} \frac{\Delta\mu}{2} \left[\begin{array}{l} \left(\frac{3}{16} c_\mu\Theta_S - \frac{\mu}{4}\frac{\Delta\lambda}{\Delta\mu}\right)r^2+\frac{1}{3}\Theta_{root}r^3+\frac{1}{4}\Theta_{tw}r^4 \\ +\left[\frac{3}{8}c_\mu\Theta_{root}r^2+\left(\frac{1}{2}\Theta_S+\frac{c_\mu}{4}\Theta_{tw}-\frac{1}{3}\frac{\Delta\lambda}{\Delta\mu}\right)r^3\right]\sin\psi \\ -\left[\left(\frac{1}{4}c_\mu\Theta_S-\frac{\mu}{4}\frac{\Delta\lambda}{\Delta\mu}\right)r^2+\frac{1}{3}\Theta_{root}r^3+\frac{1}{4}\Theta_{tw}r^4\right]\cos2\psi \\ -\left[\frac{c_\mu}{8}\Theta_{root}r^2+\frac{1}{6}\left(\Theta_S+\frac{c_\mu}{2}\Theta_{tw}\right)r^3\right]\sin3\psi \\ +\frac{1}{16}c_\mu\Theta_S r^2\cos4\psi \end{array}\right]_{r_{low}(i_{reg})}^{r_{up}(i_{reg})} d\psi \qquad (25)$$

Here, all parts symmetric to the y-axis do not contribute, i.e. the steady part and terms containing $\sin\psi, \cos2\psi, \sin3\psi$ and $\cos4\psi$ can be eliminated. It remains to solve

For the longitudinal flapping moment, the multiplication of Eq. (21) with $\cos\psi$ results in

$$\Delta\overline{M}_{\beta}^{(c1)}\cos\psi = \frac{\Delta\mu}{2}\int_{r_{low}}^{r_{up}} \left[\begin{array}{l} \left(\frac{c_\mu}{8}\Theta_C r-\frac{1}{2}\beta_0 r^2\right)+\left(\frac{1}{2}\Theta_C r^2-\frac{\mu_0}{4}\beta_0 r\right)\sin\psi \\ +\left[\frac{c_\mu}{4}\Theta_{root}r+\left(\frac{1}{2}\Theta_S+\frac{c_\mu}{4}\Theta_{tw}-\frac{\Delta\lambda}{\Delta\mu}\right)r^2\right]\cos\psi \\ +\left[\left(\frac{c_\mu}{4}\Theta_S-\mu\frac{1}{2}\frac{\Delta\lambda}{\Delta\mu}\right)r+\Theta_{root}r^2+\Theta_{tw}r^3\right]\sin2\psi \\ -\frac{1}{2}\beta_0 r^2\cos2\psi+\left(\frac{1}{2}\Theta_C r^2-\frac{\mu_0}{4}\beta_0 r\right)\sin3\psi-\frac{c_\mu}{8}\Theta_S r\sin4\psi \\ -\left[\frac{c_\mu}{4}\Theta_{root}r+\frac{1}{2}\left(\Theta_S+\frac{c_\mu}{2}\Theta_{tw}\right)r^2\right]\cos3\psi-\frac{c_\mu}{8}\Theta_C r\cos4\psi \end{array}\right] dr \qquad (26)$$

$$\Delta\overline{M}_{\beta C}^{(c1)} = \frac{1}{\pi}\sum_{i_{reg}=1}^{N_{reg}} \int_{\psi_{beg}(i_{reg})}^{\psi_{end}(i_{reg})} \frac{\Delta\mu}{2} \left[\begin{array}{l} \left[\frac{c_\mu}{8}\Theta_{root}r^2+\left(\frac{1}{6}\Theta_S+\frac{c_\mu}{2}\Theta_{tw}-\frac{1}{3}\frac{\Delta\lambda}{\Delta\mu}\right)r^3\right]\cos\psi \\ +\left[\left(\frac{c_\mu}{8}\Theta_S-\mu\frac{1}{4}\frac{\Delta\lambda}{\Delta\mu}\right)r^2+\frac{1}{3}\Theta_{root}r^3+\frac{1}{4}\Theta_{tw}r^4\right]\sin2\psi \\ -\left[\frac{c_\mu}{8}\Theta_{root}r^2+\left(\frac{1}{6}\Theta_S+\frac{c_\mu}{12}\Theta_{tw}\right)r^3\right]\cos3\psi \\ -\frac{c_\mu}{16}\Theta_S r^2\sin4\psi \end{array}\right]_{r_{low}(i_{reg})}^{r_{up}(i_{reg})} d\psi \qquad (27)$$

The same procedure is now applied to the contribution of the flapping motion, based on Eq. (22), with $\cos\psi, \sin2\psi, \cos3\psi$ and $\sin4\psi$ being removed.

$$\Delta\overline{M}_{\beta 0}^{(c2)} = \frac{1}{2\pi}\sum_{i_{reg}=1}^{N_{reg}} \int\limits_{\psi_{beg}(i_{reg})}^{\psi_{end}(i_{reg})} -\frac{\Delta\mu}{2}\left[\left(\frac{1}{3}r^3\cos 2\psi + \frac{c_\mu}{8}r^2(\sin\psi+\sin 3\psi)\right)\Delta\beta_C\right]_{r_{low}(i_{reg})}^{r_{up}(i_{reg})} d\psi \tag{28}$$

Multiplication of Eq. (22) with $\sin\psi$ results in

$$\Delta\overline{M}_{\beta}^{(c2)}\sin\psi = -\frac{\Delta\mu}{2}\int\limits_{r_{low}}^{r_{up}} \begin{bmatrix} \left(\frac{1}{2}r^2\sin 2\psi + r\frac{c_\mu}{4}(\cos\psi-\cos 3\psi)\right)\Delta\beta_0 \\ +\left(\frac{1}{2}r^2(\cos\psi-\cos 3\psi) + r\frac{c_\mu}{8}(2\sin 2\psi - \sin 4\psi)\right)\Delta\beta_S \\ +\left(\frac{1}{2}r^2(-\sin\psi+\sin 3\psi) + r\frac{c_\mu}{8}(1-\cos 4\psi)\right)\Delta\beta_C \end{bmatrix} dr \tag{29}$$

Using the same simplifications from above the lateral flapping moment results in

$$\Delta\overline{M}_{\beta S}^{(c2)} = \frac{1}{\pi}\sum_{i_{reg}=1}^{N_{reg}} \int\limits_{\psi_{beg}(i_{reg})}^{\psi_{end}(i_{reg})} -\frac{\Delta\mu}{2}\left[\left(\frac{1}{6}r^3(-\sin\psi+\sin 3\psi) + r^2\frac{c_\mu}{16}(1-\cos 4\psi)\right)\Delta\beta_C\right]_{r_{low}(i_{reg})}^{r_{up}(i_{reg})} d\psi \tag{30}$$

For the longitudinal flapping moment the multiplication of Eq. (22) with $\cos\psi$ results in

$$\Delta\overline{M}_{\beta}^{(c2)}\cos\psi = -\frac{\Delta\mu}{2}\int\limits_{r_{low}}^{r_{up}} \begin{bmatrix} \left(\frac{1}{2}r^2(1+\cos 2\psi) + r\frac{c_\mu}{4}(\sin\psi+\sin 3\psi)\right)\Delta\beta_0 \\ +\left(\frac{1}{2}r^2(\sin\psi+\sin 3\psi) + r\frac{c_\mu}{8}(1-\cos 4\psi)\right)\Delta\beta_S \\ +\left(\frac{1}{2}r^2(\cos\psi+\cos 3\psi) + r\frac{c_\mu}{8}(2\sin 2\psi + \sin 4\psi)\right)\Delta\beta_C \end{bmatrix} dr \tag{31}$$

All parts symmetric to the y-axis do not contribute, i.e. the steady part and terms with $\sin\psi, \cos 2\psi, \sin 3\psi$ and $\cos 4\psi$ can be eliminated.

$$\Delta\overline{M}_{\beta C}^{(c2)} = \frac{1}{\pi}\sum_{i_{reg}=1}^{N_{reg}} \int\limits_{\psi_{beg}(i_{reg})}^{\psi_{end}(i_{reg})} -\frac{\Delta\mu}{2}\left[\left(\frac{1}{6}r^3(\cos\psi+\cos 3\psi) + r^2\frac{c_\mu}{16}(2\sin 2\psi+\sin 4\psi)\right)\Delta\beta_C\right]_{r_{low}(i_{reg})}^{r_{up}(i_{reg})} d\psi \tag{32}$$

Only $\Delta\beta_C$ contributes to aerodynamic flapping moments in the coefficients a_{ij} of Eq. (12). This is not surprising since β_0 does not contribute to the thrust, therefore $\Delta\beta_0$ as well does not contribute to the flapping moment. The perturbation itself is a strip in longitudinal direction only, parallel to the x-axis. The lateral flapping motion with $\Delta\beta_S$ generates maximum angles of attack at 0 and 180 deg azimuth due to its maximum angular velocity reached there. At 90 and 270 deg, where it reaches its maximum upper and lower deflections, the angle of attack is zero. Only $\Delta\beta_C$ generates maximum velocities perpendicular to the disk and therefore maximum angles of attack at 90 and 270 deg azimuth. The angles of attack add to the slipstream velocities and generate perturbation lift and moment contributions. Now all contributions to the flapping equation Eq. (13) are at hand to put them together fro

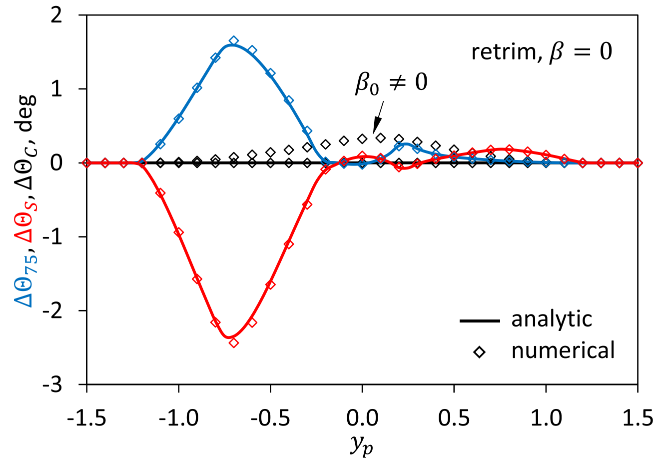

Fig. 3. Rotor controls required to retrim a rotor in a propeller slipstream.

$$\begin{bmatrix} \nu_\beta^2 & 0 & -\gamma\Delta\overline{M}_{\beta 0}^{(c2)} \\ 0 & \nu_\beta^2-1 & -\gamma\left(\Delta\overline{M}_{\beta S}^{(b)} + \Delta\overline{M}_{\beta S}^{(c2)}\right) \\ -\gamma\Delta\overline{M}_{\beta C}^{(b)}(\Delta\beta_0) & -\gamma\Delta\overline{M}_{\beta C}^{(b)}(\Delta\beta_S) & \nu_\beta^2 - 1 - \gamma\Delta\overline{M}_{\beta C}^{(c2)} \end{bmatrix}\begin{Bmatrix}\Delta\beta_0\\ \Delta\beta_S\\ \Delta\beta_C\end{Bmatrix} = \gamma\begin{Bmatrix}\Delta\overline{M}_{\beta 0}^{(a)} + \Delta\overline{M}_{\beta 0}^{(c1)} \\ \Delta\overline{M}_{\beta S}^{(a)} + \Delta\overline{M}_{\beta S}^{(c1)} \\ \Delta\overline{M}_{\beta C}^{(a)} + \Delta\overline{M}_{\beta C}^{(c1)}\end{Bmatrix} \tag{33}$$

Analytic expressions can be derived for all contributions $\Delta\overline{M}_\beta$. Subsequently, the matrix equation can be solved for the flapping perturbations $\overrightarrow{\Delta\beta}$ directly by inversion of the system matrix $\mathbf{A}$ at the left and multiplication with the excitation vector $\vec{c}$ on the right. Formally this can be written as

$$\mathbf{A}\overrightarrow{\Delta\beta} = \vec{c} \quad\Rightarrow\quad \overrightarrow{\Delta\beta} = \mathbf{A}^{-1}\vec{c} \tag{34}$$

Alternatively, the contributions $\Delta\overline{M}_{\beta 0,S,C}$ can be computed by numerical integration over r and ψ. Then, the flapping perturbations $\Delta\beta_{0,S,C}$ have to be systematically varied until the equation is fulfilled, i.e. until the error is minimum.

$$\left(\nu_\beta^2\Delta\beta_0 - \gamma\Delta\overline{M}_{\beta_0}\right)^2 + \left[\left(\nu_\beta^2-1\right)\Delta\beta_S - \gamma\Delta\overline{M}_{\beta_S}\right]^2 + \left[\left(\nu_\beta^2-1\right)\Delta\beta_C - \gamma\Delta\overline{M}_{\beta_C}\right]^2 = 0 \tag{35}$$

3. Results and discussion

The following investigations are of interest:

- Trim of the rigid rotor (no blade motion) in undisturbed air to specified values of thrust and hub moment coefficients C_T, C_{Mx}, C_{My} at prescribed operating conditions: μ_∞, α_S. This was part of Ref. [7]. A new result is the trim with rotor coning β_0 included.
- Retrim with the propeller slipstream sweeping laterally across the rotor disk. This keeps thrust and hub moment coefficients constant, and with it the induced and overall inflow ratio λ_{i0}, λ. This was also part of Ref. [7]. A new result is presented by the trim with included rotor coning to identify perturbations $\Delta\beta_0$ relative to the coning in undisturbed air of the first item above.
- New result: Without retrim, evaluate the variations $\Delta C_T, \Delta C_{Mx}$, $\Delta C_{My}, \Delta\lambda_{i0} = \Delta\lambda$ of the rigid rotor (no flapping) and with flapping

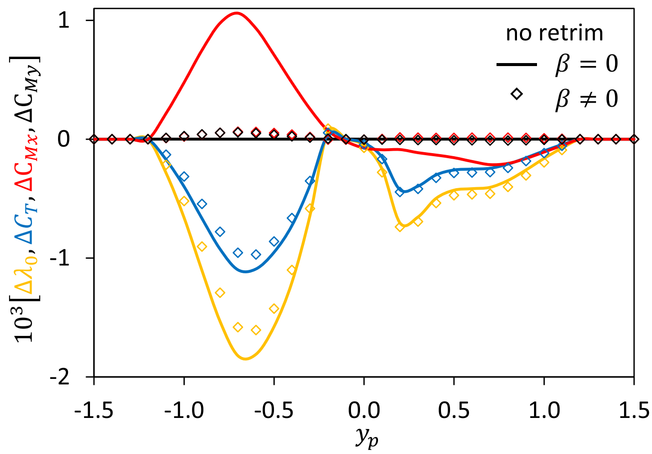

Fig. 4. Rotor thrust, moment, and inflow perturbations caused by a propeller slipstream.

due to the propeller slipstream sweeping laterally across the rotor disk.

- New result: Without retrim, compute the perturbations in blade flapping $\Delta\beta_0, \Delta\beta_S, \Delta\beta_C$ that develop due to the propeller slipstream sweeping laterally across the rotor disk.

Recall results from Ref. [7] with operational data as given therein, addressing the first two items: $\mu_\infty = 0.3084, \alpha_S = -12$ deg, $C_T = 0.00995, C_{Mx} = C_{My} = 0$. The propeller slipstream within the rotor disk has a width of $\Delta y = 0.448$ of the rotor radius and an additional advance ratio of $\Delta\mu_\infty = 0.1283$, see Table 3 and Table 4. Note that the slipstream perturbation amounts to ca. 40 % of the speed of flight.

3.1. Trim of the rigid rotor in undisturbed air

The rotor trim results in undisturbed air without coning β_0 are computed by the analytical and the numerical model. Results with coning are obtained by numerical solution and all these results are compared in Table 5. Differences are in the order of 1 per mille and can be attributed to the radial and azimuthal discretization of the numerical solution. Including the rotor coning requires a lateral control angle Θ_C, which is positive when β_0 is included. This is because the upward coning causes an upwash and hence a lift leading to an upward flapping moment in the forward blade position, relative to the rigid rotor without coning. In the rear position, these effects are reversed. That contribution to the blade normal velocity is $\Delta U_P(\beta_0) = \mu_0 \cos\psi \sin\beta_0$, see Eq. (2). This

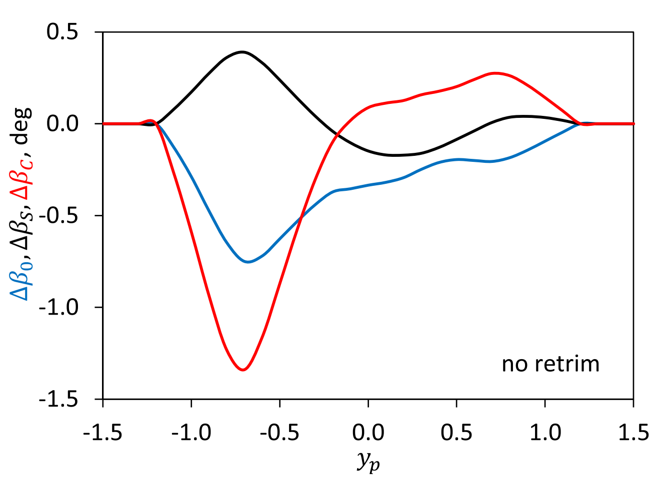

Fig. 5. Rotor blade flapping perturbations caused by a propeller slipstream.

can only be compensated by a positive control angle Θ_C. It should be noted that without coning the same effect would evolve, when using an inflow model with a longitudinal gradient superimposed to its mean value used here. In that case, the induced velocity field includes an upwash (relative to the mean) in the front of the disk and an additional downwash (relative to the mean) in the rear part. This requires a positive control angle Θ_C to eliminate its impact on the aerodynamic pitching moment.

3.2. Trim of the rigid rotor subjected to the slipstream

The rotor remains in the same operational condition, but now including the slipstream perturbation. Subject of investigation are the control angle perturbations relative to the undisturbed trim that are required to reject the perturbation impact on the trim (rotor thrust and hub moments). The results shown in Fig. 3 compare the analytic solution (lines, evaluated at a resolution of $\Delta y_p = 0.05$) with the one obtained numerically (symbols, $\Delta y_p = 0.1$). y_p is the mean slipstream position relative to the hub center. It is positive for slipstream interactions on the advancing side and negative for those on the retreating side. The numerical solution was computed using 20 blade elements and 2 deg azimuth increments, where the retrim with coning β_0 is also included. Note that $\Delta\Theta_{75}$ and $\Delta\Theta_S$ do not change with or without inclusion of β_0.

The small controls required to mitigate the slipstream effects for interactions on the advancing side observed in the right half of Fig. 3 are caused by the increased dynamic pressure. A pure increase of it would generate more lift there, but this is widely compensated by reduced angles of attack due to the rotor inflow, which is increased in the same proportion as the advance ratio. Also, the high dynamic pressure only requires small pitch control angles to generate large lift and aerodynamic rolling moments. The control sensitivity for interactions on the advancing side is increased and consequently only small perturbations in control angles are required to reject the slipstream impact on thrust and hub moments.

For slipstream positions on the retreating side (left side of Fig. 3), however, the significant loss of dynamic pressure is further exaggerated by the increased inflow. Both effects lead to a significant loss of retreating side lift with a developing associated aerodynamic rolling moment. Due to the low dynamic pressure, the sensitivity of the control angles on the retreating side becomes rather small and large changes of control angles are required to regain the rotor trim. In addition, the large coupling of collective control with longitudinal control in fast forward flight finally leads to large increase of the collective control angle. This requires even a larger amount of longitudinal cyclic control angles. Because the flight condition already requires large collective and longitudinal cyclic control angles, these additional ones may eventually be limited by the mechanical hard stops of the control range.

For the rigid rotor the lateral control angle remains zero both in undisturbed air or with the propeller slipstream included. This is due to the symmetry of air loads with respect to the rotor y-axis, i.e., the lift in the front of the disk is the same as in the rear. Including coning, for the reasons mentioned before, a lateral cyclic control angle $\Delta\Theta_C$ is required (black open symbols). It is maximum for the center position of the slipstream, due to the cosine in $\Delta U_P(\beta_0) = \mu_0 \cos\psi \sin\beta_0$, which becomes largest for $\psi = 0$ or 180 deg, i.e. around the central position $y_p = 0$.

3.3. Aerodynamic perturbations of the rotor trim due to the slipstream

The third item addresses the variations of thrust and hub moment coefficients as well as the induced inflow ratio without retrim of the rotor, that develop due to the propeller slipstream as shown in Fig. 4. Lines denote results without flapping $\beta = \beta_0 = 0$; symbols represent results with flapping. For the rigid rotor ($\beta = \beta_0 = 0$) the pitching moment ΔC_{My} remains unaffected due to the symmetry of lift with respect to the y-axis. Similar to the control angles required to retrim, the thrust ΔC_T (blue) and especially the rolling moment coefficients ΔC_{Mx} (red) show largest perturbations for slipstream positions on the retreating side of the disk for the reasons explained before. Because it is originated by the thrust, the mean inflow ratio $\Delta\lambda_0$ (yellow) follows the same trend as ΔC_T.

When including blade flapping (symbols in Fig. 4), the coning and the cyclic flapping is developing, the latter being excited by the harmonic part of the rolling moment ΔC_{Mx}. Because of the small hinge offset of 4.1 % rotor radius the natural frequency of flapping is 1.03/rev, i.e. the phase lag of the flapping response is little less than 90 deg. Therefore, the flapping upward motion significantly reduces the angles of attack where the slipstream increases it and vice versa. For the aerodynamics, the consequences on thrust and with it, the induced inflow variations are small. Compared to the rigid rotor, slightly less magnitude is resulting. The largest impact of flapping motion is a significant reduction of the aerodynamic rolling moment to the same order of magnitude shown by the pitching moment (red symbols essentially follow the black symbols). Therefore, the flapping motion degree of freedom significantly reduces the aerodynamic hub moments developing, compared to the rigid rotor.

3.4. Rotor blade flapping perturbations due to the slipstream

The fourth item of the list deals with the blade flapping (coning and first harmonic motion) developing when no retrim of the rotor is performed. Due to the aerodynamic perturbations caused by the slipstream and the air loads caused by the steady and harmonic flapping, the steady and dynamic flapping response is given in Fig. 5. The coning $\Delta\beta_0$ (blue) mainly follows the trend of the thrust ΔC_T shown in Fig. 4. But it is also depending on the mean radial distribution of lift along the radius and thus shows some deviations from the thrust curve, especially for slipstream positions around the hub center.

Longitudinal flapping $\Delta\beta_C$ (red) is largest for slipstream positions on the retreating side. As seen in Fig. 4, the largest rolling moment (positive: advancing side up) causes the largest flapping deflection almost 90 deg later, i.e. at 180 deg azimuth, which is a negative value of longitudinal flapping. This is reversed for slipstream positions on the advancing side. Overall, the curve of $\Delta\beta_C$ appears nearly as a mirrored curve of ΔC_{Mx} in Fig. 4.

Lateral flapping $\Delta\beta_S$ (black) is largest where the pitching moment, ΔC_{Mx} in Fig. 4, is also largest, i.e. for slipstream positions on the retreating side. This appears nonphysical, because a positive pitching moment (i.e., nose-up) would result in the largest flapping deflection almost 90 deg later, i.e. around 270 deg azimuth, which is a negative value for $\Delta\beta_S$. Here, the contribution from the large rolling moment dominates over the small one from the pitching moment, leading to the result shown in Fig. 5.

4. Conclusions

In this article the analytical solution of propeller slipstream interaction with a helicopter rotor is further extended to include the flapping degree of freedom for the first time. Results for controls required to reject the slipstream perturbations on thrust and hub moments are shown without and with rotor blade flapping. Major conclusions are:

- With the propeller slipstream the local air speed is increased by ca. 40 % of the flight speed, locally exceeding the V_{NE} of the helicopter.
- Because the helicopter rotor is significantly tilted nose-down in fast forward flight, the propeller slipstream also increases the local inflow normal to the rotor disk. Within the slipstream the rotor thrust-induced velocity is therefore reduced.
- The pilot controls to reject the rotor trim perturbations caused by the propeller slipstream are small for slipstream positions on the advancing side. This can be attributed to the high sensitivity of local lift to pilot controls in the high dynamic pressure area.
- The pilot control angles required for retrimming the rotor are large for slipstream positions on the retreating side. This is due to low sensitivity of local lift to pilot controls in the reduced dynamic pressure area. The total rotor controls may reach mechanical limits in this case, because the rotor trim in undisturbed air already requires large collective and cyclic control angles.
- The introduction of rotor blade flapping alleviates the aerodynamic perturbations. Especially due to cyclic flapping the rolling moment is reducing.
- Therefore, it appears advisable to approach the refueling position with the advancing side of the rotor near the propeller slipstream, and not with the retreating side near to it.
- When retrimming the rotor to zero cyclic flapping, the coning is still varying due to the propeller slipstream contribution to normal velocities. The maximum coning angle is obtained for a slipstream position in the rotor center.

CRediT authorship contribution statement

Berend G. van der Wall: Writing – review & editing, Writing – original draft, Visualization, Validation, Project administration, Investigation, Formal analysis.

Declaration of competing interest

The authors declare that they have no known competing financial interests or personal relationships that could have appeared to influence the work reported in this paper.

Data availability

No data was used for the research described in the article.

Funding

This work was performed by institutional funding of DLR within the project URBAN-Rescue.

Acknowledgements

The Author thanks Patrick Löchert of the DLR Institute of Aerodynamics and Flow Technology in Braunschweig for provision of the graph in Fig. 1 as well as Thomas Jann and Sven O. Schmidt of the DLR Institute of Flight Systems in Braunschweig for provision of operational data and information on the F(AI)^{2}R project of DLR.

Appendix

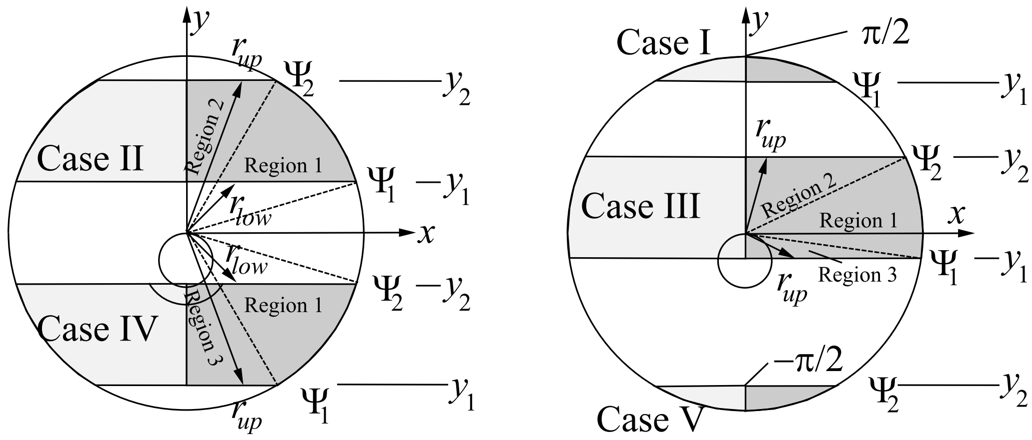

(a) Cases II and IV (b) Cases I, III, and V

Fig. 6. Azimuthal and radial regions of integration for different cases.

Table 1
Technical data of the tanker aircraft and its propeller.

Parameter	Symbol	Unit	Value
Maximum take-off mass	MTOM	t	141
Minimum speed	V_{min}	km/h, m/s	230(*), 63.9
Number of propellers	N_p		4
Number or propeller blades	N_{bp}		8
Propeller radius	R_p	m	2.67
Blade chord length	c_p	m	0.5*
Propeller solidity	σ_p,		0.477*
Propeller tilt angle	$\Delta\alpha_p$	deg	-2

* = estimated

Table 2
Technical data of the helicopter rotor.

Parameter	Symbol	Unit	Value
Maximum take-off mass	MTOM	t	19.5
Maximum speed	V_{NE}	km/h, m/s	295, 82
Number of rotor blades	N_b		6
Rotor radius	R	m	11
Blade chord length	c	m	0.74
Rotor solidity	σ		0.128
Blade twist	Θ_{tw}	deg/R	-6.0

(*) = estimated

Table 3
Operational condition for a representative air-to-air refueling situation.

Parameter	Symbol	Unit	Value
Height above sea level	h	m	2130
Temperature	T_∞	°C	1.16
Air density	ρ_∞	kg/m^3	0.9933
Speed of sound	a_∞	m/s	332.6
Flight speed	V_∞	m/s	65.71
Flight Mach number	M_∞		0.1976
Aircraft mass	m_{airc}	t	130.0
Aircraft angle of attack	α_{airc}	deg	11.65
Glide ratio w. flaps	ϵ		6.68(*)
Propeller thrust	T_p	kN	47.73
Rotational speed	Ω_p	rad/s	88.2
Blade tip speed	$(\Omega R)_p$	m/s	235.5

(*continued on next page*)

Table 3 (*continued*)

Parameter	Symbol	Unit	Value
Tip Mach number	$M_{tip,p}$		0.708
Helicopter mass	m_{hel}	t	17.0
Rotor disk tilt angle	α_S	deg	-12.0*
Rotational speed	Ω	rad/s	19.37
Blade tip speed	ΩR	m/s	213.1
Tip Mach number	M_{tip}		0.641
Rotor advance ratio	μ_0		0.3017

* = estimated

Table 4
Propeller slipstream data and perturbations acting on the rotor.

Parameter	Symbol	Unit	Value
Slipstream contraction ratio	R_∞/R_p		0.9228
Slipstream width ratio	$2R_\infty/R$		0.4480
Slipstream velocity	ΔV_∞	m/s	27.35
Perturbation advance ratio	$\Delta\mu$		0.1255
Inflow ratio perturbation	$\Delta\lambda$		0.0218
Combined inflow & advance ratio perturbation	$\Delta_{\mu\lambda}$		0.0194

Table 5
Helicopter trim in undisturbed flow without and with blade coning.

Solution method	Θ_{75}, deg	Θ_S, deg	Θ_C, deg	β_0, deg
Analytical	12.31	-6.26	0.0	0.0
Numerical	12.32	-6.27	0.0	0.0
Ditto + β_0	12.32	-6.27	2.04	5.3

The different possibilities of the slipstream covering parts of the rotor disk are defined in Table 6 and sketched in Fig. 6.

Table 6
Case selection.

Case	Explanation: the slipstream…
I	overlaps with the advancing edge of the rotor, see Fig. 6 (b)
II	is within the advancing side of the rotor disk, see Fig. 6 (a)
III	overlaps with the rotor center, see Fig. 6 (b)
IV	is within the retreating side of the rotor disk, see Fig. 6 (a)
V	overlaps with the retreating edge of the rotor, see Fig. 6 (b)

The different regions of integration shown in Fig. 6 are defined in Table 7.

Table 7
Radial and azimuthal integration bounds for all regions of all cases.

Case	y_1	y_2	ψ_1	ψ_2	N_{reg}	Region	r_{low}	r_{up}	ψ_{beg}	ψ_{end}
I	$\geq 0,\ <1$	≥ 1	$\tan^{-1}\frac{y_1}{\sqrt{1-y_1^2}}$	n.a.	1	1	$\frac{y_1}{\sin\psi}$	1	ψ_1	$\frac{\pi}{2}$
II	$\geq 0,\ <y_2$	$>y_1,\ <1$	$\tan^{-1}\frac{y_1}{\sqrt{1-y_1^2}}$	$\tan^{-1}\frac{y_2}{\sqrt{1-y_2^2}}$	2	1	$\frac{y_1}{\sin\psi}$	1	ψ_1	ψ_2
						2	$\frac{y_1}{\sin\psi}$	$\frac{y_2}{\sin\psi}$	ψ_2	$\frac{\pi}{2}$
III	$<0,\ >-1$	$>0,\ <1$	$\tan^{-1}\frac{y_1}{\sqrt{1-y_1^2}}$	$\tan^{-1}\frac{y_2}{\sqrt{1-y_2^2}}$	3	1	0	1	ψ_1	ψ_2
						2	0	$\frac{y_2}{\sin\psi}$	ψ_2	$\frac{\pi}{2}$
						3	0	$\frac{y_1}{\sin\psi}$	$-\frac{\pi}{2}$	ψ_1
IV	$<y_2,\ >-1$	$\leq 0,\ >y_1$	$\tan^{-1}\frac{y_1}{\sqrt{1-y_1^2}}$	$\tan^{-1}\frac{y_2}{\sqrt{1-y_2^2}}$	2	3	$\frac{y_2}{\sin\psi}$	$\frac{y_1}{\sin\psi}$	$-\frac{\pi}{2}$	ψ_1
						1	$\frac{y_2}{\sin\psi}$	1	ψ_1	ψ_2
V	≤ -1	$\leq 0,\ >-1$	n.a.	$\tan^{-1}\frac{y_2}{\sqrt{1-y_2^2}}$	1	1	$\frac{y_2}{\sin\psi}$	1	$-\frac{\pi}{2}$	ψ_2

References

[1] H.P. Dunn, The USAF CH-3C helicopter V/STOL in-flight refueling program and its operational uses and implications, 22nd Annual Forum and Technology Display of the American Helicopter Society, Washington, D.C., May 11-13, 1966.
[2] B.E. Kashawlic, J.G. Irwin-III, J.S. Bender, M. Schwerke, MH-47G DAFCS helicopter aerial refueling control laws, 67th Annual Forum and Technology Display of the American Helicopter Society, Virginia Beach, VA, May 3-5, 2011.
[3] P.R. Thomas, U. Bhandari, S. Bullock, T.S. Richardson, J.L. du Bois, Advances in air to air refuelling, Progr. Aerospace Sci 71 (2014) 14–35, https://doi.org/10.1016/j.paerosci.2014.07.001.
[4] S.O. Schmidt, M. Jones, P. Löchert, Evaluation of a real-time simulation environment for helicopter air-to-air refuelling investigations, Aeronaut. J 127 (2023) 754–772, https://doi.org/10.1017/aer.2022.106.
[5] P. Löchert, S.O. Schmidt, T. Jann, M. Jones, Consideration of tanker's wake flow for helicopter air-to-air refueling, AIAA Aviation Forum, Virtual, Aug. 2-6, 2021. https://doi.org/10.2514/6.2021-2561.
[6] B.G. van der Wall, L.B. van der Wall, Analytical estimate of rotor controls required for a straight vortex disturbance rejection, J. Am. Helicopter Society 62 (2017) 015001, https://doi.org/10.4050/JAHS.62.015001, 1-4.
[7] B.G. van der Wall, Analytical estimate of rotor controls required for a propeller wake disturbance rejection, J. Am. Helicopter Society 69 (2024) 045011, https://doi.org/10.4050/JAHS.69.045011, 1-6.
[8] W.Z. Stepniewski, C.N. Keys, Rotary-Wing Aerodynamics, Dover Publications, Inc., Mineola, NY, 1984, Chapter 3.2. ISBN: 9780486646473.
[9] J.G. Leishman, Principles of Helicopter Aerodynamics, Cambridge University Press, New York, NY, 2000, Chapters 2.3 and 2.4. ISBN: 9780521660600.